

Journal of Materials Chemistry A

Accepted Manuscript



This is an *Accepted Manuscript*, which has been through the Royal Society of Chemistry peer review process and has been accepted for publication.

Accepted Manuscripts are published online shortly after acceptance, before technical editing, formatting and proof reading. Using this free service, authors can make their results available to the community, in citable form, before we publish the edited article. We will replace this *Accepted Manuscript* with the edited and formatted *Advance Article* as soon as it is available.

You can find more information about *Accepted Manuscripts* in the [Information for Authors](#).

Please note that technical editing may introduce minor changes to the text and/or graphics, which may alter content. The journal's standard [Terms & Conditions](#) and the [Ethical guidelines](#) still apply. In no event shall the Royal Society of Chemistry be held responsible for any errors or omissions in this *Accepted Manuscript* or any consequences arising from the use of any information it contains.

Cite this: DOI: 10.1039/c0xx00000x

www.rsc.org/xxxxxx

ARTICLE TYPE

Preparation of Porous (Ni,Co)₃(BO₃)₂/Ni(OH)₂ Nanosheet networks as Pseudocapacitor Materials with Superior Performance

Yuanzhen Chen,^{a,b} Yongning Liu^{*a} and Wei Yan^{*b}*Received (in XXX, XXX) Xth XXXXXXXXX 20XX, Accepted Xth XXXXXXXXX 20XX*

DOI: 10.1039/b000000x

Abstract: A porous (Ni,Co)₃(BO₃)₂/Ni(OH)₂ composite was prepared by one step chemical deposition in a mild condition. The morphology and structure observation showed that the porous flocculence structures were built by ultrathin nanosheets which consist of amorphous structure and nanocrystals in size of 1-3 nm. The porous structure displays a large specific surface area of 237 m²·g⁻¹ which is rare value for nickel and cobalt compounds. Cyclic voltammetry and galvanostatic charge–discharge tests show that specific capacitance of 1982 and 1445 F·g⁻¹ at 0.5A·g⁻¹ and 10 A·g⁻¹ have been achieved respectively. After 1000 cycles, the capacitance retention reached up to 93.6% at a current density of 5 A·g⁻¹.

Introduction

With the increasing demand for energy and growing concerns about air pollution and global warming, it is urgent to find alternative energy sources to store and converse energy. Therefore, Li-ion batteries, fuel cells, and supercapacitors¹ have been researched widely to make a sustainable development. Among these new energy devices, supercapacitors are considered as a promising candidate for energy storage due to high specific capacitance, long cycle life, and low maintenance cost. Generally, supercapacitors are classified into electrical double-layer capacitors and pseudocapacitors depending on charge storage mechanism. Due to the high demand of large specific capacitances, pseudocapacitors had been paid much attention. Transition metal oxides such as RuO₂,^{2,3} MnO₂,⁴⁻⁶ Co₃O₄,^{7,8} or Co(OH)₂,⁹ NiO or Ni(OH)₂¹⁰⁻¹² and their composites^{13,14} are qualified to be electrochemical capacitor materials. Though noble oxide RuO₂ exhibits remarkably high specific capacitance values ranging from 720 to 760 F·g⁻¹ (for a single electrode),^{15,16} the high cost of these materials limits their commercial applications. The nickel or cobalt oxides and their hydroxides have been paid more attention to for their huge theoretical capacitance (e.g. NiO-2573 F·g⁻¹,¹ Ni(OH)₂-2365 F·g⁻¹,¹⁷ Co₃O₄-3560 F·g⁻¹). However, the electrode materials usually can not fully release their theoretical capacity for some reasons, such as big particle size and low conductivity, therefore measured capacitances generally range from 300 to 700 F·g⁻¹.¹⁸ To reduce particle size, many methods have been employed to prepare the nanoscale materials.¹⁹ Growing ultrathin mesoporous nanosheet arrays of electrode materials (e.g. Co₃O₄ or Ni(OH)₂) on the Ni foam support is a good method.^{8,9,14,20} An unique 3D electrode manifests exceptional supercapacitive performance with ultrahigh specific capacitance at high current densities and excellent cycling stability. To improve conductivity, graphene was

composited with active materials, and also made big contribution in both capacitance and cycle life.^{11,21,22} In addition, compositing different electrode materials can promote capacitive property. Li et al. prepared doughnut-like nanostructured Ni(OH)₂-Co(OH)₂ composites and had obtained big capacitance improvement compared with Ni(OH)₂.¹⁷ Authors attributed the enhancement of the overall electrochemical performances to the synergetic contribution of Ni(OH)₂ and Co(OH)₂. Also another composites such as CoMoO₄-NiMoO₄·xH₂O¹³, Mn₃O₄-Co₃O₄²³ and Co(OH)₂/Ni/Si-MCPs²⁴ displayed some increases in the capacitances and cycle life. However, generally they needed multi-step process to prepare and their yield also was limited.

Except for the electrode materials mentioned above, metal borates can be used as electrode material of capacitor but correlation research is rare. Gao et al had synthesized a kind of metal borate (Ni₃(BO₃)₂ nanoribbons), but its specific capacitance only was 170 F·g⁻¹.²⁵ In this paper, we will introduce a novel porous (Ni,Co)₃(BO₃)₂/Ni(OH)₂ composites prepared in one step chemical precipitation method and got a large specific capacitance and high capacitance retention.

Experimental

Synthesis of porous (Ni,Co)₃(BO₃)₂/Ni(OH)₂ composites and pH values measurement

Firstly, Cobalt chloride (CoCl₂·6H₂O) (0.025 mol) and nickel chloride (NiCl₂·6H₂O) (0.025 mol) were dissolved in 50 ml deionized water and then heated the mixture solution to 80 °C. Another 50 ml of KBH₄ (0.01 mol) solution was dropped into above solution for 1 h with an assistance of appropriate mechanical stirring. The product was filtered and washed 5 times using deionized water. In this process, the pH values of reacting solution and filtered solution were measured by a pH meter (Sartorius, PB-10), and then green product was dried at 80 °C for

12 h.

Characterization methods

The morphology of sample was observed using a field emission scanning electron microscope (FESEM, JSM-6700F) and high-resolution transmission electron microscopy (HRTEM, JEM-2100F). X-ray diffraction (XRD) analysis was carried out on an XpertPRO X-ray diffractometer with Cu K α radiation ($\lambda=0.15444$ nm). Nitrogen adsorption-desorption measurements were carried out on ASAP 2020 surface area and porosity analyzer. The elemental surface composition of the samples was analyzed by X-ray photoelectron spectroscopy (XPS, AXIS ultra DLD).

Electrochemical measurements

The electrode was prepared as follows: the mass of active electrode material was 16 mg. Active electrode material, super P (conductive carbon nanoparticles) and polytetrafluoroethylene (PTFE) (5 wt% of water suspension) were mixed in a mass ratio of 80:15:5 and then suspended in ethanol. After ultrasonic dispersion, the mixture was heated to evaporate most of the ethanol and to form a plasticine-like slurry, and then it was smeared onto a nickel foam current collector (2 cm²) of which the average mass was 53 mg. After drying overnight at 80 °C under vacuum, it was pressed at a pressure of 6 MPa into an electrode.

The Cyclic voltammetry (CV) measurements were carried out on an electrochemistry Workstation (Princeton Applied Research PARSTAT 2273) in a three-electrode system in a solution of 6 M KOH at room temperature, in which platinum foil and Hg/HgO electrodes were used as counter and reference electrodes respectively. Galvanostatic charge-discharge (GCD) measurement in a range of 0.1-0.475 V was also carried out in three-electrode system, and the specific capacitance, energy density and power density were calculated from the discharge process of GCD in three electrode system according to equation (1), (2) and (3) respectively:^{26, 27}

$$C_m = \frac{I \times t}{\Delta V \times m} \quad (1)$$

$$E = \frac{1}{2} \times C_m \times (\Delta V)^2 \quad (2)$$

$$P = \frac{E}{t} \quad (3)$$

where C_m is the specific capacitance of the electrode (F g⁻¹); m is the mass of active material in one electrode (g); I is the discharge current (A); t is the discharge time (s); ΔV is the potential window (V); E is energy density (Wh kg⁻¹) and P is power density (kW kg⁻¹).

To match the capacitance of both electrode, the capacitor cells were assembled in an asymmetrical structure using 10 mg of sample (Ni:Co=1:1) and 85 mg of activated carbon (AC) as positive and negative respectively. GCD and cycle-life were measured by a battery testing system (Neware TC-3008W, Neware technology limited, China) in a potential range of 0.2-1 V by different current densities. The electrolyte was 6 M KOH and tests were performed at ambient temperature (298 K). The specific capacitance of the composite was evaluated from the discharge process according to equation (4):

$$C_m = \frac{2I \times t}{\Delta V \times m} \quad (4)$$

where C_m was the specific capacitance of the electrode (F g⁻¹), m was the mass of active material in one electrode (g), I was the discharge current (A), t was the discharge time (s), and ΔV was the potential window (V). The factor of 2 comes from the fact that the total capacitance measured from the test cells in the sum of two equivalent single electrode capacitors in series. It should be stated that the specific capacitance of positive active electrode material and negative AC electrode had been tested at 0.5 Ag⁻¹ and they were 1982 and 233 Fg⁻¹ respectively. Herein, $C_{AC(-)}=233$ Fg⁻¹ × 0.085 g = 19.81 F, and $C_{\text{active electrode (+)}}=1982$ Fg⁻¹ × 0.01 g = 19.82 F. According to the equation: $1/C_{\text{total}}=1/C_{AC(+)}+1/C_{\text{active electrode (+)}}$, when $C_{AC(-)}=C_{\text{active electrode (+)}}$, $C_{\text{active electrode (+)}}=1/2 C_{\text{total}}$. Therefore, the factor of 2 appeared in equation (4).

Results and discussion

The powder XRD data of the samples (pristine sample and the one after heat treatment at 850 °C for 2h in Ar atmosphere) are shown in **figure 1**. The pristine sample mainly shows an amorphous structure except for two small broad diffraction peaks at 33.5° and 60.5°, matching the strongest (121) and moderately strong (330) diffraction peaks of orthorhombic M₃(BO₃)₂ (M=Co and Ni). In order to analyze the components of the amorphous pristine sample clearly, the sample after heat treatment at 850 °C had been analyzed. Except for M₃(BO₃)₂, only nickel monoxide (NiO) but no cobalt oxide has been found. NiO should be produced by the decomposition of Ni(OH)₂ and no Co(OH)₂ exists in the pristine amorphous sample. Therefore, Co should exist in a form of Co₃(BO₃)₂, but whether Ni₃(BO₃)₂ exists in the pristine sample is not confirmed by XRD analysis.

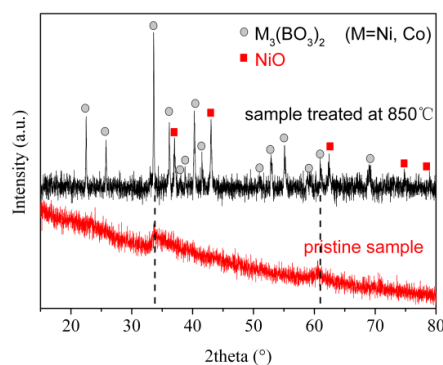


Figure 1 XRD patterns of the pristine sample (red line) and the samples treated at 850 °C for 2h (black line).

Surface element analysis was carried out using XPS to determine the compositions of the pristine sample (**figure 2**). The atomic ratio of surface element (Ni:Co:B) calculated from XPS analysis is 1.29 : 1.1 : 1.09. Herein, the atomic ratio of Co:B ~ 1:1 is not consistent with that of Co₃(BO₃)₂ (Co:B=3:2). It can be inferred that excess element B should exist in Ni₃(BO₃)₂. Figure 2a shows the B XPS spectra and only one broad peak with binding energies of 192.18 eV is observed for the B 1s level, which is assigned to the (BO₃) group.²⁸ In addition, another peak of O 1s at 531.2 eV is assigned to OH groups (figure 2d).^{29, 30} To

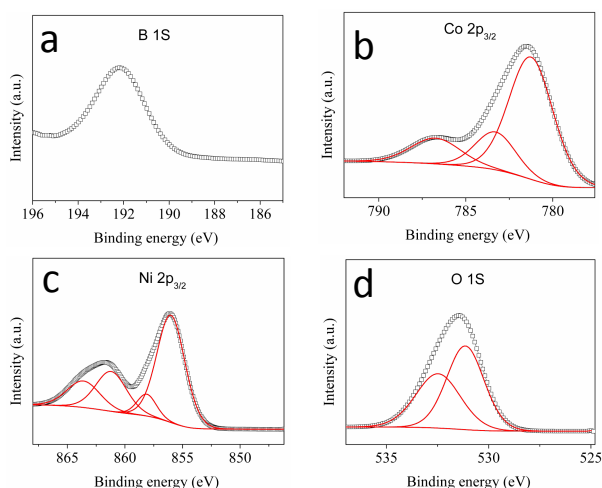


Figure 2 XPS spectrum of (a) B, (b) Co, (c) Ni and (d) O

the both metals, the high binding energy indicates that there is no metallic Ni and Co or their oxides (figure 2b, c). According to the above analysis, it can be confirmed that the components of the pristine sample are $\text{Ni}_3(\text{BO}_3)_2$, $\text{Ni}(\text{OH})_2$ and $\text{Co}_3(\text{BO}_3)_2$ respectively. herein, The pristine sample with a mole ratio of Ni:Co=1:1 is defined as $(\text{Ni},\text{Co})_3(\text{BO}_3)_2/\text{Ni}(\text{OH})_2$.

It is well known that hydrolysis of KBH_4 is spontaneous and then makes the pH value of solution increase intensely. The reaction equations are as follows:³¹



The equation (5) and (6) show that the increase of pH is attributed to the hydrolysis of BH_4^- , which was confirmed by a measured pH value of 10.28 after KBH_4 hydrolysis. With the increase of pH value, Co^{2+} and Ni^{2+} will precipitate into a green composite of $\text{Ni}(\text{OH})_2$, $\text{Ni}_3(\text{BO}_3)_2$, and $\text{Co}_3(\text{BO}_3)_2$. When the reaction finished, the colorless filtrate was collected and its pH value was 10.22 suggesting that Co^{2+} and Ni^{2+} ion had precipitated fully.

Figure 3a shows a field-emission scanning electron microscope (FESEM) image of porous $(\text{Ni},\text{Co})_3(\text{BO}_3)_2/\text{Ni}(\text{OH})_2$ composite. It can be observed that the sample shows a flocculence morphology. As can be seen from the higher-magnification FESEM image (figure 3b), this flocculence morphology consists of ultra-thin nanosheets which interconnect each other and form a flocculence networks with a highly open and porous structure, and most of the nanosheets surface is highly accessible to the electrolyte when they are used as an electrode for ECs. Therefore, morphology greatly affects the specific capacitance. For Ni/Co composite materials, the nanosheets usually achieve larger specific capacitance than nanowires and nanorods, and have good capacitance retention (see table S1, figure S1(a, b) supporting information). This ultrathin feature is further verified by the typical nanosheets image observed from the transmission electron microscope (TEM). The selected-area electron diffraction pattern (the inset in figure 3c) shows various diffraction cycles characteristic of the amorphous structures,

indicating the $(\text{Ni},\text{Co})_3(\text{BO}_3)_2/\text{Ni}(\text{OH})_2$ composite has poor crystallinity. The high-resolution TEM (HRTEM) image shown in figure 3d reveals that the nanosheet consists of nanocrystals and amorphous phases. The nanocrystals are very small and their sizes are mainly in a range of 1-3 nm, but their largely different crystal orientations and many amorphous phases make $(\text{Ni},\text{Co})_3(\text{BO}_3)_2/\text{Ni}(\text{OH})_2$ composite show amorphous diffraction rings. Seeing from N_2 adsorption-desorption isotherm shown in figure 3e, a distinct hysteresis loop is observed with typical IV sorption behavior, indicating the existence of a typical mesoporous microstructure. The pore-size-distribution curve (the inset in Fig. 3e) shows that there mainly are small mesopores in the range of 2.5-5 nm. The mesoporous structure gives rise to a relatively high Brunauer-Emmett-Teller (BET) specific surface area (SSA) of $237 \text{ m}^2\text{g}^{-1}$ and a big pore volume of $0.532 \text{ cm}^3\text{g}^{-1}$ calculated by Barrett-Joyner-Halenda (BJH) model. This SSA value is larger than that of mostly other metal oxide or hydroxide used in pseudocapacitance,^{1, 9, 13, 23, 32-34} mostly below $120 \text{ m}^2\text{g}^{-1}$ (see table S2, figure S1b, supporting information). Such characteristics of the sample permit easy access for ions to the electrode/electrolyte interface, which is crucial for surface redox reactions.^{34, 35} The features mentioned above closely are related to the preparation method. Usually the electrode materials (e.g. $\text{Co}(\text{OH})_2$, $\text{Ni}(\text{OH})_2$) made by general method such as chemical

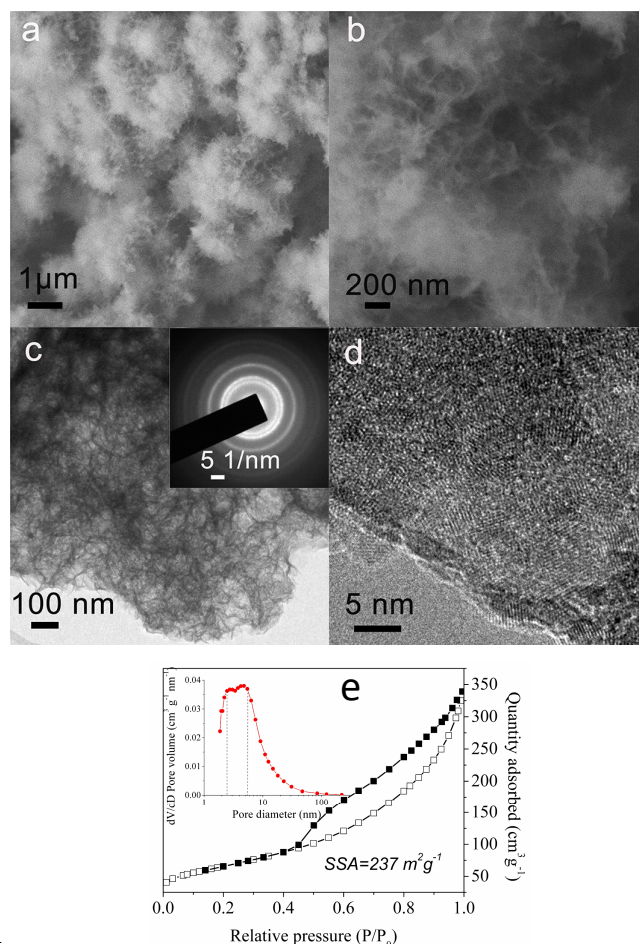


Figure 3 (a, b) SEM and (c, d) TEM images of sample. (e) N_2 adsorption/desorption isotherm of sample at 77 K and (inset) the porosity distribution calculated by BJH model.

precipitation and hydrothermal method are compact. However, the formation of the flocculence network with high porosity closely relates to the hydrogen gas released by the KBH_4 . In the reacting process, the continuously encouraged hydrogen gas can promote pores forming.

In this work, another two samples had been prepared to determine which composites with different mole ratio of Ni:Co (design proportion) obtain the best capacitance performance. In order to evaluate the influence of assistant material (Ni foam, super P and PTFE) on the performance of active electrode materials, the CV curve of Ni foam loaded super P and PTFE was measured, and the result showed that its CV curve almost displayed a line (**figure 4a**) indicating its ignorable influence on performance of active electrode materials. To compare the electrochemical reactivity of these three active materials, CV tests were performed in three electrode system. Figure 4(a, b) demonstrate the CV and GCD curves of three samples tested at $5\text{mV}\cdot\text{s}^{-1}$ and $0.5\text{ A}\cdot\text{g}^{-1}$, respectively. It is clearly seen that the redox potential are different (figure 4a) and the specific capacitance has a very close relationship with the mole ratio of

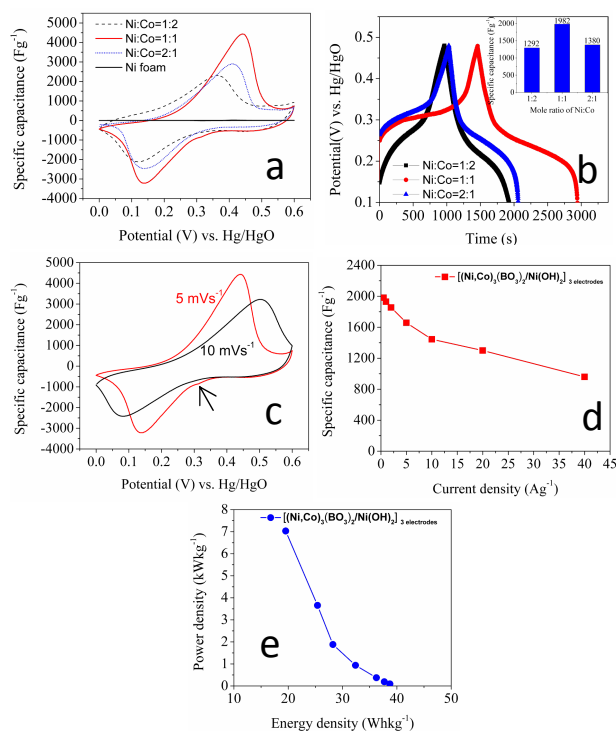


Figure 4 (a) CV curves (scanning rate: $5\text{mV}\cdot\text{s}^{-1}$) and (b) charge-discharge curves (current density: $0.5\text{ A}\cdot\text{g}^{-1}$) of Ni foam and samples ($n_{\text{Ni}}:n_{\text{Co}}=1:2$, $1:1$ and $2:1$); (c) CV curves (5 and $10\text{ mV}\cdot\text{s}^{-1}$), (d) specific capacitance versus current densities and (e) Ragone plot (power density vs. energy density) of $(\text{Ni},\text{Co})_3(\text{BO}_3)_2/\text{Ni}(\text{OH})_2$ composite (sample $n_{\text{Ni}}:n_{\text{Co}}=1:1$). All electrochemical measurements in this figure were performed using three-electrode configuration.

Ni:Co (figure 4b). There is an appropriate ratio corresponding to the maximum specific capacitance (inset of figure 4b), namely the sample with a Ni:Co mole ratio of $1:1$ obtained the biggest specific capacitance reaching up to $1982\text{ F}\cdot\text{g}^{-1}$. Therefore, the following analyses are related to this sample with a Ni:Co mole ratio of $1:1$, and it is named as $(\text{Ni},\text{Co})_3(\text{BO}_3)_2/\text{Ni}(\text{OH})_2$ composite.

Figure 4c shows the CV curves of $(\text{Ni},\text{Co})_3(\text{BO}_3)_2/\text{Ni}(\text{OH})_2$ composite at 5 and $10\text{ mV}\cdot\text{s}^{-1}$. For both curves, a pair of redox peaks can be observed. Clearly, the interval of redox peaks increase with the increase of scanning rates. At related low scanning rate of $5\text{ mV}\cdot\text{s}^{-1}$, the oxidation and reduction peaks appear 0.44 V and 0.14 V , respectively. But the both peaks shifts to 0.5 and 0.075 V respectively when the scanning rate at $10\text{ mV}\cdot\text{s}^{-1}$. The redox delays at high scanning rate.^{17, 24, 36} The detailed electrochemical reactions and corresponding discussion are displaying in supporting information (see **figure S2, supporting information**).

The specific capacitances of the electrodes were measured by means of GCD test in three electrode system. Figure 4(d) shows the specific capacitances of $(\text{Ni},\text{Co})_3(\text{BO}_3)_2/\text{Ni}(\text{OH})_2$ composite measured at various current densities from 0.5 to $40\text{ A}\cdot\text{g}^{-1}$. With the increase of current density, the specific capacitance of $(\text{Ni},\text{Co})_3(\text{BO}_3)_2/\text{Ni}(\text{OH})_2$ composite decrease slowly. The specific capacitance is 1930 , 1855 , 1658 , 1445 and $1300\text{ F}\cdot\text{g}^{-1}$ at the current density of 1 , 2 , 5 , 10 and $20\text{ A}\cdot\text{g}^{-1}$ respectively. Even the current density reaches up to $40\text{ A}\cdot\text{g}^{-1}$, its capacitance still retains $960\text{ F}\cdot\text{g}^{-1}$. The Ragone plot of energy density versus power density for $(\text{Ni},\text{Co})_3(\text{BO}_3)_2/\text{Ni}(\text{OH})_2$ composite derived from charge-discharge curves is displayed in figure 4e. At a power density of $100\text{ W}\cdot\text{kg}^{-1}$, the sample obtains an energy density of $39\text{ Wh}\cdot\text{kg}^{-1}$, while the power density increases to $7000\text{ W}\cdot\text{kg}^{-1}$, the energy density still retains $20\text{ Wh}\cdot\text{kg}^{-1}$. These results indicate that $(\text{Ni},\text{Co})_3(\text{BO}_3)_2/\text{Ni}(\text{OH})_2$ composite developed in the present study is a very promising positive electrode material for high performance supercapacitors.

The CV curve of $(\text{Ni},\text{Co})_3(\text{BO}_3)_2/\text{Ni}(\text{OH})_2$ composite as negative electrode was tested for its relatively big SSA value. The result shows that it displays slant rectangular shape and has no clear redox peaks (see **figure S3, supporting information**) indicating that its capacitance is mainly contributed by double-layer capacitor. However, compared with the pseudocapacitance, its double-layer specific capacitance is only $33\text{ F}\cdot\text{g}^{-1}$. Therefore, when it is used as positive electrode, most of capacitance is contributed by pseudocapacitance.

In the electrochemical reaction, which component of $(\text{Ni},\text{Co})_3(\text{BO}_3)_2/\text{Ni}(\text{OH})_2$ mainly provides pseudocapacitance has been discussed as follows. XPS test results show the atom ratio of Ni:Co:B is $1.29:1.1:1.09$, and the calculated mole ratio of $\text{Co}_3(\text{BO}_3)_2:\text{Ni}_3(\text{BO}_3)_2:\text{Ni}(\text{OH})_2$ is $2:1:4$, then the mass percentage of $\text{Ni}(\text{OH})_2$ and $(\text{Ni},\text{Co})_3(\text{BO}_3)_2$ is $29.7\text{ wt}\%$ and $70.3\text{ wt}\%$ respectively. According to the reference,³⁷ the theoretic specific capacitance is $2082\text{ F}\cdot\text{g}^{-1}$ for $\text{Ni}(\text{OH})_2$. If all capacitance is only contributed by $\text{Ni}(\text{OH})_2$, even though its specific capacitance reaches the theoretic value, its contributed specific capacitance is only $618\text{ F}\cdot\text{g}^{-1}$ ($2082\times 29.7\%$ $\text{F}\cdot\text{g}^{-1}$) which is less than total value of $1982\text{ F}\cdot\text{g}^{-1}$. Therefore, another $1364\text{ F}\cdot\text{g}^{-1}$ is contributed by $(\text{Ni},\text{Co})_3(\text{BO}_3)_2$. It is clearly seen that $(\text{Ni},\text{Co})_3(\text{BO}_3)_2$ proves high pseudocapacitance.

To evaluate the cycle performance of $(\text{Ni},\text{Co})_3(\text{BO}_3)_2/\text{Ni}(\text{OH})_2$ composite, the capacitor cells were assembled in a asymmetrical structure using $(\text{Ni},\text{Co})_3(\text{BO}_3)_2/\text{Ni}(\text{OH})_2$ composite as positive and AC as negative respectively.

In order to match the capacitance of two electrodes, the GCD and cycle-life tests of commercial AC ($\text{SSA}=2000\text{ m}^2\cdot\text{g}^{-1}$) at a

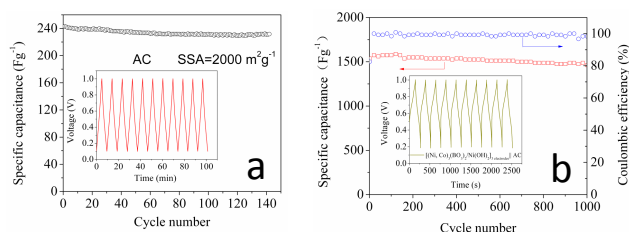


Figure 5 (a) cycling performance of AC at the current densities of $0.5 \text{ A}\cdot\text{g}^{-1}$ test in symmetrical structure (inset is the initial 10 charge-discharge curves of the composite at $0.5 \text{ A}\cdot\text{g}^{-1}$). (b) cycling performance of asymmetrical structure of $(\text{Ni},\text{Co})_3(\text{BO}_3)_2/\text{Ni}(\text{OH})_2$ composite and AC at the current densities of $5 \text{ A}\cdot\text{g}^{-1}$ (inset is the initial 10 charge-discharge curves of the composite at $5 \text{ A}\cdot\text{g}^{-1}$).

current of $0.5 \text{ A}\cdot\text{g}^{-1}$ was carried out in a symmetrical structure, and its average specific capacitance after 140 cycles was $233 \text{ F}\cdot\text{g}^{-1}$, as shown in **figure 5a**. Then 10 mg of $(\text{Ni},\text{Co})_3(\text{BO}_3)_2/\text{Ni}(\text{OH})_2$ composite and 85 mg of AC were used to fabricate an asymmetrical capacitor device and it was measured in a voltage range from 0.2 to 1V (inset of figure 5b). The long-cycle test were carried out and the results show that the specific capacitance of $(\text{Ni},\text{Co})_3(\text{BO}_3)_2/\text{Ni}(\text{OH})_2$ composite retains $1474 \text{ F}\cdot\text{g}^{-1}$ from initial value of $1574 \text{ F}\cdot\text{g}^{-1}$ after 1000 cycles at $5 \text{ A}\cdot\text{g}^{-1}$. The capacitance retention is 93.6% (figure 5b). After cycling at high current densities for a long time, the composites still show good electrochemical reversibility with about 100% coulombic efficiency for each charge-discharge cycle.

There are some reasons for the high specific capacitance and capacitance retention for amorphous $(\text{Ni},\text{Co})_3(\text{BO}_3)_2/\text{Ni}(\text{OH})_2$ composites. Firstly, the ultrathin nanosheets morphology greatly improves the utilization of active materials. Secondly, this composite gets a big SSA value of $237 \text{ m}^2\cdot\text{g}^{-1}$ and the appropriate pore size in a range of 2.5-5 nm. All these characteristic can increase the contact area between the active materials and electrolyte, and also provide more transport channels for ions, and finally leads to faster kinetics and higher utilization of active materials at higher charge-discharge rates.³⁸

Conclusions

A flocculence morphology of amorphous porous $(\text{Ni},\text{Co})_3(\text{BO}_3)_2/\text{Ni}(\text{OH})_2$ composite was prepared by a simple chemical precipitation method. HRTEM showed that the ultrathin sheet of sample consisted of amorphous structure and nanocrystal in size of 1-3 nm, for which the active material could react with OH^- ions easily, and resulted in a large specific capacitance and high capacitance retention. The specific capacitance of $(\text{Ni},\text{Co})_3(\text{BO}_3)_2/\text{Ni}(\text{OH})_2$ composite reached up to $1982 \text{ F}\cdot\text{g}^{-1}$ at a current density of $0.5 \text{ A}\cdot\text{g}^{-1}$. When the current density increased to $40 \text{ A}\cdot\text{g}^{-1}$, its specific capacitance still kept $960 \text{ F}\cdot\text{g}^{-1}$. After 1000 cycles at $5 \text{ A}\cdot\text{g}^{-1}$. The capacitance retention was 93.6%. In addition, this amorphous structure gave the sample a large specific surface area (SSA) of $237 \text{ m}^2\cdot\text{g}^{-1}$ and high pore volume of $0.53 \text{ cm}^3\cdot\text{g}^{-1}$ with pore size distribution of 2-5 nm. The large SSA and appropriate pore size increased the contact area between electrolyte and active material and also provide more transport channels for ions. Therefore, It also obtained high specific energy density of $39 \text{ Wh}\cdot\text{kg}^{-1}$ at power density of $100 \text{ W}\cdot\text{kg}^{-1}$. Even the

power density increased to $7000 \text{ W}\cdot\text{kg}^{-1}$, the energy density still retained $20 \text{ Wh}\cdot\text{kg}^{-1}$.

Acknowledgements

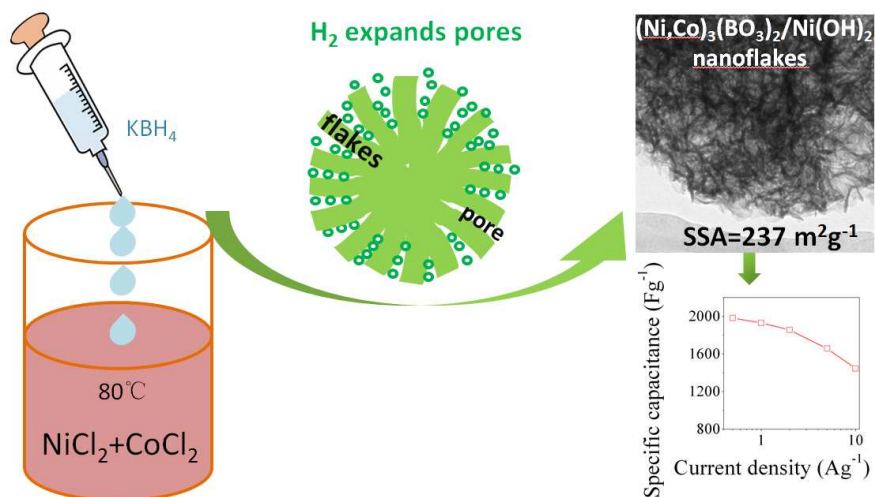
This work was supported by the China Postdoctoral Science Foundation (No. 2012M521760).

Notes and references

- ^a State Key Laboratory for Mechanical Behavior of Materials, School of Material Science and Engineering, Xi'an Jiaotong University, Xianning west road No. 28, Xi'an 710049, PR China
TEL: +86-29-82664602
E-mail: ynliu@mail.xjtu.edu.cn
- ^b School of Energy and Power Engineering, Xi'an Jiaotong University, Xianning west road No. 28, Xi'an 710049, PR China
TEL: +86-29-82664731
E-mail: yanwei@mail.xjtu.edu.cn
- † Electronic Supplementary Information (ESI) available: Ni and Co composited materials with large capacitance and good capacitance retention; comparison on specific surface area and capacitance for Co_3O_4 and other Ni/Co composites with different morphologies; the corresponding electrochemical reactions when $(\text{Ni},\text{Co})_3(\text{BO}_3)_2/\text{Ni}(\text{OH})_2$ composite was used as positive and negative electrode material. See DOI: 10.1039/b000000x/
- H. Pang, B. Zhang, J. Du, J. Chen, J. Zhang and S. Li, *RSC Adv.*, 2012, **2**, 2257.
 - R. R. Bi, X. L. Wu, F. F. Cao, L. Y. Jiang, Y. G. Guo and L. J. Wan, *J. Phys. Chem. C*, 2010, **114**, 2448.
 - Z. S. Wu, D. W. Wang, W. Ren, J. Zhao, G. Zhou, F. Li and H. M. Cheng, *Adv. Funct. Mater.*, 2010, **20**, 3595.
 - A. J. Roberts and R. C. T. Slade, *Electrochim. Acta*, 2010, **55**, 7460.
 - L. Hu, W. Chen, X. Xie, N. Liu, Y. Yang, H. Wu, Y. Yao, M. Pasta, H. N. Alshareef and Y. Cui, *ACS Nano*, 2011, **5**, 8904.
 - Y. Cheng, S. Lu, H. Zhang, C. V. Varanasi and J. Liu, *Nano Lett.*, 2012, **12**, 4206.
 - Y. Wang, Z. Zhong, Y. Chen, C. Ng and J. Lin, *Nano Res.*, 2011, **4**, 695.
 - Y. Gao, S. Chen, D. Cao, G. Wang and J. Yin, *J. Power Sources*, 2010, **195**, 1757.
 - C. Yuan, L. Yang, L. Hou, L. Shen, X. Zhang and X. W. Lou, *Energy Environ. Sci.*, 2012, **5**, 7883.
 - J. Y. Kim, S.-H. Lee, Y. Yan, J. Oh and K. Zhu, *RSC Adv.*, 2012, **2**, 8281.
 - H. Wang, H. S. Casalongue, Y. Liang and H. Dai, *J. Am. Chem. Soc.*, 2010, **132**, 7472.
 - X.-h. Xia, J.-p. Tu, X.-l. Wang, C.-d. Gu and X.-b. Zhao, *J. Mater. Chem.*, 2011, **21**, 671.
 - M. C. Liu, L. B. Kong, C. Lu, X. J. Ma, X. M. Li, Y. C. Luo and L. Kang, *J. Mater. Chem. A*, 2013, **1**, 1380.
 - Z. Lu, Q. Yang, W. Zhu, Z. Chang, J. Liu, X. Sun, D. Evans and X. Duan, *Nano Res.*, 2012, **5**, 369.
 - S. H. Oh and L. F. Nazar, *J. Mater. Chem.*, 2010, **20**, 3834.
 - Y. Xie and D. Fu, *Mater. Chem. Phys.*, 2010, **122**, 23.
 - J. Li, M. Yang, J. Wei and Z. Zhou, *Nanoscale*, 2012, **4**, 4498.
 - X. Wang, A. Sumboja, E. Khoo, C. Yan and P. S. Lee, *J. Phys. Chem. C*, 2012, **116**, 4930.

- 19 R. B. Rakhi, W. Chen, D. Cha and H. N. Alshareef, *Nano Lett.*, 2012, **12**, 2559.
- 20 G. Hu, C. Li and H. Gong, *J. Power Sources*, 2010, **195**, 6977.
- 21 A. Chidembo, S. H. Aboutaleb, K. Konstantinov, M. Salari, B. Winton, S. A. Yamini, I. P. Nevirkovets and H. K. Liu, *Energy Environ. Sci.*, 2012, **5**, 5236.
- 22 X. C. Dong, H. Xu, X. W. Wang, Y. X. Huang, M. B. Chan-Park, H. Zhang, L. H. Wang, W. Huang and P. Chen, *ACS Nano*, 2012, **6**, 3206.
- 23 H. Pang, J. Deng, J. Du, S. Li, J. Li, Y. Ma, J. Zhang and J. Chen, *Dalton Trans.*, 2012, **41**, 10175.
- 24 M. Li, S. Xu, T. Liu, F. Wang, P. Yang, L. Wang and P. K. Chu, *J. Mater. Chem. A*, 2013, **1**, 532.
- 25 H. Pang, Q. Lu, C. Chen, X. Liu and F. Gao, *J. Mater. Chem.*, 2011, **21**, 13889.
- 26 W. Zhou, X. Cao, Z. Zeng, W. Shi, Y. Zhu, Q. Yan, H. Liu, J. Wang and H. Zhang, *Energy Environ. Sci.*, 2013, **6**, 2216.
- 27 P.-C. Chen, G. Shen, Y. Shi, H. Chen and C. Zhou, *ACS Nano*, 2010, **4**, 4403.
- 28 E. Z. Kurmaev, V. V. Fedorenko, V. R. Galakhov, S. Bartkowski, S. Uhlenbrock, M. Neumann, P. R. Slater, C. Greaves and Y. Miyazaki, *J. Supercond.*, 1996, **9**, 97.
- 29 C. Zhang, C. Feng, P. Zhang, Z. Guo, Z. Chen, S. Li and H. Liu, *RSC Adv.*, 2012, **2**, 1643.
- 30 J. Yang, H. Liu, W. N. Martens and R. L. Frost, *J. Phys. Chem. C*, 2010, **114**, 111.
- 31 G. N. Glavee, K. J. Klabunde, C. M. Sorensen and G. C. Hadjipanayis, *Langmuir*, 1993, **9**, 162.
- 32 S. Zhang, J. Li, T. Wen, J. Xu and X. Wang, *RSC Adv.*, 2013, **3**, 2754.
- 33 H. Wang, Q. Gao and L. Jiang, *Small*, 2011, **7**, 2454.
- 34 D.-W. Wang, F. Li and H.-M. Cheng, *J. Power Sources*, 2008, **185**, 1563.
- 35 Y. Li, B. Tan and Y. Wu, *J. Am. Chem. Soc.*, 2006, **128**, 14258.
- 36 Z. A. Hu, Y. L. Xie, Y. X. Wang, H. Y. Wu, Y. Y. Yang and Z. Y. Zhang, *Electrochim. Acta*, 2009, **54**, 2737.
- 37 J. Yan, Z. Fan, W. Sun, G. Ning, T. Wei, Q. Zhang, R. Zhang, L. Zhi and F. Wei, *Adv. Funct. Mater.*, 2012, **22**, 2632.
- 38 X. H. Xia, J. P. Tu, Y. Q. Zhang, Y. J. Mai, X. L. Wang, C. D. Gu and X. B. Zhao, *J. Phys. Chem. C*, 2011, **115**, 22662.

40



Hydrogen expanded $(\text{Ni,Co})_3(\text{BO}_3)_2/\text{Ni}(\text{OH})_2$ nanoflakes into porous structure and thereby made it obtain a big SSA and superior pseudocapacitor performance.